Michigan State University

National Superconducting Cyclotron Laboratory

COULOMB DISPLACEMENT ENERGY AND THE LOW-ENERGY ASTROPHYSICAL S_{17} FACTOR FOR THE $^{7}Be(p,\gamma)^{8}Be$ REACTION

B.A. BROWN, A. CSOTO, and R. SHERR

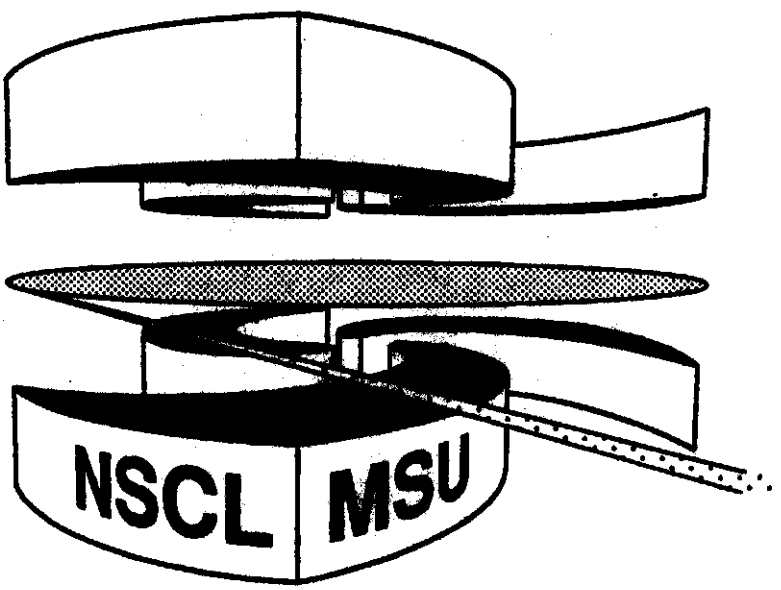

MSUCL-984

JULY 1995

Coulomb Displacement Energy and the Low-Energy Astrophysical S_{17} Factor for the $^{7}Be(p,\gamma)^{8}B$ Reaction

B. A. Brown

National Superconducting Cyclotron Laboratory and Department of Physics *and Astronomy*

Michigan *State* University, *East* Lansing, *MI 48824-1321*

A. Csótó

National Superconducting *Cyclotron Laboratory*

Michigan *State* University, *East* Lansing, MI *48824-1321*

R . Sherr

Department of Physics, Princeton University, *Princeton, New Jersey 08544*

Abstract

The relationship between the Coulomb displacement energy for the A=8, $J=2^{+}$, T=l state and the low-energy astrophysical S_{17} factor for the $^{7}Be(p,\gamma)^{8}B$ reaction is discussed. The displacement energy is interpreted in a particle-hole model. The dependence of the particle displacement energy on the potential well geometry is investigated and is used to relate the particle displacement energy to the rms radius and the asymptotic normalization of the valence proton wave function in ^{8}B. The asymptotic normalization is used to calculate the astrophysical S_{17} factor for the $^{7}Be(p,\gamma)$ reaction. The relationship to the $^{7}Li(n,\gamma)$ reaction, the ^{8}B quadrupole moment, radial density, and break-up momentum distribution are also discussed.

Typeset using REVTEX

I. INTRODUCTION

Measurements of high energy solar neutrinos in the Homestake[1] and Kamiokande II and III[2] experiments have found a significantly smaller number of solar neutrinos compared to that expected from the standard solar model.[3] The ^{8}B β^+ decay is the main source of these these high energy solar neutrinos. ^{8}B is formed by the ^{7}Be(p,γ)^{8}B reaction at a center of mass energy of about 20 keV. Its cross section is conventionally expressed in terms of the S_{17} factor.[3] S_{17} is known only from an extrapolation of data at energies above 100 keV. Also the highest precision data disagree, with those of Parker[4] and Kavanagh et al.[5] being about 30 percent higher than those of Filippone et al.[6] and Vaughn et al..[7] This has lead to the investigation of other ways to determine the S_{17} factor such as the Coulomb dissociation,[8] as well as other properties of ^{8}B which are indirectly related to the S_{17} factor such as its total reaction cross section,[9] quadrupole moment,[10] and break-up momentum distribution.[11]

Much of the theoretical work has been based upon using a potential model to generate the single-particle wave function for the most loosely bound proton, and then combining this with a shell-model calculation of the spectroscopic factor to obtain the asymptotic normalization of the wave function. This current work was initiated by the observation that the potential model parameters (e.g. the radius R and diffuseness a of the Woods-Saxon potential) used in previous calculations are taken from some "standard" sets based upon nucleon-nucleus scattering optical potential analyses, and that these "standard" parameters were not obviously appropriate to the particular case of ^{7}Be plus protons. We thus investigated the extent to which the potential parameters could be determined from the displacement energy of the A=8, $J^\pi=2^+$, T=1 state as given by the binding energy difference between the ^{8}B and ^{8}Li ground states. In addition, we also examined several quantities of related interest including the ^{7}Li(n,γ) cross section, the Q moment, the density distributions, and the momentum distributions.

II. COULOMB DISPLACEMENT ENERGY

The relationship between the root-mean-square (rms) radius of the valence proton and the displacement energy is well known.[12,13] Qualitatively, the larger the rms radius the smaller the displacement energy since the valence proton is further from the core protons. This leads to the Thomas-Ehrman effect in which loosely bound valence nucleons have a relatively smaller displacement energy compared to more tightly bound nucleons. In addition, for a fixed binding energy, nucleons in a low ℓ state have a smaller displacement energy compared to those in a high ℓ state because the centrifugal barrier for high ℓ results in a smaller rms radius. For heavier nuclei (A>16) with a relatively simple shell-model configuration, many quantitative calculations of the displacement energy have been carried out. At the beginning of the 0d1s shell (A=17, T=1/2) and the 0f1p shell (A=41, T=1/2), the observed displacement energy is found to be about 10 percent larger than that obtained from calculations which involve only the lowest shell-model configuration together with the Coulomb interaction. These cases include those for high ℓ values whose Coulomb shift is not very sensitive to the potential-well geometry. This "Nolen-Schiffer" (NS) anomaly appears not to have a simple explanation but is due to a combination of core-polarization, high-order configuration mixing, and charge-asymmetric strong interactions effects. The systematics of the displacement energies of light nuclei can also be semi-quantitatively accounted for with a simple potential-well geometry.[14]

In this paper we apply what has been learned about the displacement energy systematics to constrain the shape of the potential for the ^{7}Be plus valence proton system. The A=8, T=1 displacement energies are more complicated than the T=1/2 systems usually considered, since at least two nucleons are involved. However, the 0p shell-model wave functions predict a relatively simple structure for A=8, T=1. The spectroscopic factors (C^2S) for (A=8, 2^+, T=1) $\rightarrow$ (A=7, $3/2^-$, T=1/2) and (A=9, $3/2^-$, T=1/2) $\rightarrow$ (A=8, 2^+, T=1) are experimentally and theoretically both near unity.[15,16] Thus, ^{8}B can be considered as a proton-particle neutron-hole configuration relative to ^{8}Be. The mirror nucleus ^{8}Li is a

proton-hole neutron-particle configuration. ^{8}Be is itself "deformed" and thus exits in both the ground state and 2^+ first excited state relative to the particle-hole configuration.

The displacement energy of the particle-hole state is simply the sum of the particle and hole displacement energies (the Coulomb particle-hole interaction is zero):

$$\Delta_8 = \Delta_{hole} + \Delta_{part}, \tag{1}$$

where Δ_8 is the A=8, T=1 displacement energy (the binding energy difference between ^{8}Li and ^{8}B). In the simplest approximation Δ_{hole} is the A=7, $3/2^-$, T=1/2 displacement energy and Δ_{part} is the A=9, $3/2^-$, T=1/2 displacement energy. The experimental values are Δ_7=1.645 MeV and Δ_9=1.851 MeV which gives $\Delta_7 + \Delta_9$=3.496 MeV compared to the experimental A=8 value of Δ_8=3.540 MeV. So the simplest model works rather well. There are however several reasons why this is not exact. One is that the actual shell-model configuration is a little more complicated than just particle-hole. Also the Thomas-Ehrman effects may be significant since the proton is unbound by by 186 keV in ^{9}B and bound by 138 keV in ^{8}B.

Since we are particularly interested in the properties of the valence proton in ^{8}B we will proceed as follows. First Eq. (1) will be modified to read

$$\Delta_8 = \Delta_{hole} + \Delta'_{part} + \Delta_{sm}, \tag{2}$$

where Δ_{sm} will take into account the 0p shell-model structure beyond particle-hole. Since the hole state is relatively tightly bound, the Thomas-Ehrman shift will be small and we will take $\Delta_{hole} = \Delta_7 = 1.645$ MeV. Δ'_{part} indicates the displacement energy for the particle in ^{8}B which may differ from $\Delta_{part} = \Delta_9$ because of the Thomas-Ehrman shift.

The shell-model correction Δ_{sm} was calculated by using the Coulomb plus charge asymmetric interaction of Ormand and Brown[17] within a full 0p shell-model basis. The matrix elements were calculated with harmonic-oscillator radial wave functions. The results for the displacement energies are: $\Delta_{hole} = \Delta_7 = 1.719$ MeV, $\Delta_8 = 3.656$ MeV and $\Delta_{part} =$

$\Delta'_{part} = \Delta_9 = 1.873$ MeV. This gives $\Delta_{sm} = 64$ keV. Since harmonic-oscillator radial wave functions are used the shell-model calculation should not necessarily be in good agreement with experiment, however, it should provide an estimate for the Δ_{sm} correction. Thus the displacement energy of the A=8 particle state is

$$\Delta'_{part} = \Delta_8 - \Delta_{hole} - \Delta_{sm} = 1.831\,\mathrm{MeV}. \tag{3}$$

We are interested on how Δ'_{part} depends upon the potential geometry, and on how the potential geometry effects the rms radius and the astrophysical S_{17} factor. To investigate this we will calculate the direct part of the Coulomb shift in a Woods-Saxon geometry. This means that we calculate the single-particle binding energy with and without the one-body Coulomb potential and take the difference to obtain the Coulomb displacement energy. The Woods-Saxons potential has the usual form of central plus spin-orbit plus Coulomb terms. The central potential has the form

$$V(r) = V_o\{1 + \exp[(r - R)/a]\}^{-1}, \tag{4}$$

where R is the radius, a is the diffuseness. We use the reduced mass in the kinetic energy operator. The spin-orbit potential is the usual derivative form with the same geometry as the central (we will show below that the spin-orbit potential is not important for our analysis). The Coulomb potential is obtained from the density distribution of four tightly-bound protons (two in 0s and two in 0p) obtained with another Woods-Saxon potential which is constrained to reproduce the experimental rms charge radius [18] of 2.52 fm for ^{9}Be.

We thus investigate the dependence of the Coulomb energy, the rms radius and the astrophysical S_{17} factor on the radius R and the diffuseness a of the central potential. In all cases we vary R and a and fix V_o in order to reproduce the proton separation energy of 138 keV. We calculate the direct Coulomb displacement energy Δ_o and relate it to Δ'_{part} by making several additional corrections:

$$\Delta'_{part} = \Delta_o + \Delta_{ex} + \Delta_{so} + \Delta_{vp} + \Delta_{np} + \Delta_{NS}. \quad (5)$$

Δ_{ex} is the exchange correction. A value of Δ_{ex}=−125 keV was obtained from the harmonic-oscillator shell-model calculation for Δ_0 by comparing the results with and without the Coulomb exchange terms. The next three terms are the relativistic spin-orbit correction (Eq. 21 in Ref 12), the vacuum polarization correction (Eq. 4.23 in Ref 13) and the proton-neutron mass difference correction (Eq. 4.29 in Ref 13), respectively. Our estimates for these are −20 keV, 12 keV and 14 keV, respectively.

The Nolen-Schiffer correction, Δ_{NS} is perhaps the most uncertain. To find a value of Δ_{NS} appropriate for the 0p shell, we examine the A=13,$1/2^-$,T=1/2 displacement energy. In this case we use a Woods-Saxon geometry for ^{12}C ($R = 2.90$ fm and $a = 0.56$ fm) similar to that of Ref 19 which reproduces the ^{12}C rms charge radius and the elastic electron scattering form factor of ^{12}C. Given these constraints the ^{12}C potential geometry is well determined. The results for the A=13 displacement energy are of the form of Eq. (5) with $\Delta_o = 2.969$ MeV, $\Delta_{ex} = -271$ keV, $\Delta_{so} = 55$ keV, $\Delta_{vp} = 18$ keV and $\Delta_{np} = 20$ keV. When equated to the A=13 experimental value of $\Delta_{part} = \Delta_{exp} = 3.003$ MeV, one obtained $\Delta_{NS} = 212$ keV or $\Delta_{NS}/\Delta_o = 0.071$. We remark that Δ_o by itself is close to experiment as observed in the analysis of Ref 14, and this can also be seen in other displacement energy calculations (see Ref 20 and references therin). We are not aware of any simple or fundamental reason why the correction terms (including the exchange term) tend to cancell. We will proceed using Eq. (5) assuming that Δ_{NS} scales as Δ_o. For our A=8 case, Δ_o is about 1.80 MeV, and we will take $\Delta_{NS} = 128$ keV. Thus we arrive at the empirical value of

$$\Delta_o(\text{empirical}) = 1.822 \pm 0.026\,\text{MeV}, \quad (6)$$

with which we will compare our calculations for the direct Coulomb shift of the valence particle. (Again we note that Δ'_{part} and Δ_o are nearly equal.) The error comes from assuming

a 20 percent uncertainty in Δ_{NS} and the analysis associated with it.

We show in Table I the results for Δ_o, the rms proton radius and the density of the valence proton at $r = 10$ fm, $\rho(10\,\mathrm{fm})$, as a function of R and a. Beyond the influence of the strong interaction (about 6 fm) the shape of the radial wave function is entirely and uniquely determined by the Coulomb plus centrifugal potentials. The only quantity which depends on the potential is the asymptotic normalization as represented, for example, by the value of ρ at $r = 10$ fm. Our ρ(r) is defined by the normalization:

$$4\pi \int \rho(r) r^2 \, dr = 1. \tag{7}$$

In order to show the correlation between Δ_o, rms and $\rho(10\,\mathrm{fm})$ we plot values obtained for these quantities in pairs in Figs. 1 (Δ_o vs rms), 2 [Δ_o vs $\rho(10\,\mathrm{fm})$] and 3 [rms vs $\rho(10\,\mathrm{fm})$]. We find that there is strong correlation between them, which implies that from a knowledge of any one of them (in particular Δ_o) we can infer a range of values for the other two.

The results in Table I were obtained for a $0p_{3/2}$ valence particle. For R=2.40 fm we show the results with and without the spin-orbit potential, and from this comparison it is clear that spin-orbit potential is not important (as long as V_o is fixed from the 138 keV separation energy). Thus to a good approximation, our results apply to both $0p_{3/2}$ and $0p_{1/2}$.

The results shown in Figs. 1–3 show that there is a rather narrow band of points which relate the quantities of interest in the framework of the Woods-Saxon potential model. From Fig. 1 one finds that the value of Δ_o=1.822±0.026 MeV corresponds to a narrow range of rms valence radii from 4.3 to 4.6 fm, and from Fig. 2 one finds that the same Δ_o corresponds to $\rho(10\,\mathrm{fm})$ values in the range 6.2 to 7.8 fm^{-6}. The correlation between the rms radius and ρ shown in Fig. 3 is even more parameter independent.

The Woods-Saxon parameter set in the middle of the range allowed by our displacement energy analysis is R=2.40 fm and a=0.62 fm. This is compared in Table II with the parameters used in a number of other potential model calculations for S_{17}. The results for Δ_o, rms and $\rho(10\,\mathrm{fm})$ for the potentials in Table II are shown by the labeled crosses in Figs.

1-3. The results with Tombrello parameters (T), obtained from an optical model analysis of 180 MeV proton scattering on Li and Be by Johansson et al.,[21] are on the high side compared to ours. The Tombrello parameters were subsequently used by Aurdal[22] and Robertson.[23] Parameter set BI from Barker is in the range of our allowed values. But his modifications of the parameters (BII and BIII) needed to reproduce the ^{7}Li(n,γ) cross section (see the discussion below) are clearly outside of our range.

III. RESULTS FOR THE ASTROPHYSICAL S_{17} FACTOR

The astrophysical S_{17} factor is related to $\rho(10\,\mathrm{fm})$ in the following way. At very low energies (< 50 keV) the ^{7}Be(p,γ)^{8}B capture cross section is dominated by the E1 transition between the ^{7}Be+p scattering states and the ^{8}B ground state,[24] and it is almost exclusively determined by contributions coming form the external part of the scattering and bound state wave functions. The asymptotic behavior of the scattering states is uniquely defined (the phase shifts being the hard sphere phase shifts – practically zero), and the asymptotic part of the wave function, which describes the ^{7}Be+p relative motion in the bound state ^{8}B, is proportional to the fixed Whittaker function,

$$\psi^I_{^8\mathrm{B}}(r) = \bar{c}_I \frac{W^+_{\eta,\ell}(kr)}{r}, \quad r \to \infty, \tag{8}$$

where $I = 1, 2$ is the channel spin, r is the radial distance between ^{7}Be and p, and k is the wave number corresponding to the ^{8}B binding energy relative to the ^{7}Be+p threshold. $\bar{c}_I$ are the constants which are required to normalize the Whittaker function to the asymptotic ^{8}B wave function. Thus, at low energies the astrophysical S_{17} factor of the capture reaction,

$$S_{17}(E) = \sigma(E) E \exp\left[2\pi\eta(E)\right], \tag{9}$$

depends only on $\bar{c}$.[25,26] (here $\eta = e^2 Z_1 Z_7/\hbar v$ with $Z_1 = 1$, and $Z_7 = 4$ is the Sommerfeld parameter). From the hard sphere scattering states one obtains:

$$S_{17}(20\text{keV}) = 36.5(\bar{c}_1^2 + \bar{c}_2^2). \tag{10}$$

(The uncertainty coming mainly from the fact that the nucleon mass is not well defined in nonrelativistic quantum mechanics, is 1–2 percent. The value of the S factor at zero energy is roughly 0.4 eV-barn higher than at 20 keV.) Using this formula we can express S_{17} (in units of eV-barns) in terms of the valence proton density at any given asymptotic radius, e.g. at 10 fm,

$$S_{17}(20\,\text{keV}) = 2.99{\cdot}10^6\,\rho_{3/2}(10\,\text{fm})\;S_{3/2}\;[(\alpha_{1,3/2} + \gamma\,\alpha_{1,1/2})^2 + (\alpha_{2,3/2} + \gamma\,\alpha_{2,1/2})^2], \tag{11}$$

were the α coefficients are determined from the transformation between the $^7\text{Be}(J_i) + \ell_j = {}^8\text{B}(J_f)$ coupling and the channel-spin coupling:

$$[J_i \otimes \ell_j]^{J_f} = \sum_I \alpha_{I,j}[(J_i \otimes 1/2)^I \otimes \ell]^{J_f}, \tag{12}$$

and γ is given by the ratio:

$$\gamma = \frac{[\theta_{1/2}\;\psi_{1/2}(10\,\text{fm})]}{[\theta_{3/2}\;\psi_{3/2}(10\,\text{fm})]}. \tag{13}$$

In Eq. (13) θ_j is the $n = 0$, ℓ=1 spectroscopic amplitude and in Eqs. (11) S_j is the spectroscopic factor. The amplitudes θ_j are given by the reduced matrix elements [27] of the creation operator, a^+:

$$\theta_j(J_i, J_f) = \frac{\langle {}^8\text{B}, J_i \,||\, a^+_{j,\text{proton}} \,||\, {}^7\text{Be}, J_f\rangle}{\sqrt{2J_i + 1}}, \tag{14}$$

When θ_j is given without its J_i, J_f arguments as in Eq. (13), it corresponds to the ^{8}B ground state ($J_i = 2$) to ^{7}Be ground state ($J_f = 3/2$) value. The spectroscopic factors take into account the additional center of mass correction factor, [28] $[A_i/(A_i - 1)] = 8/7$:

$$S_j = \frac{A_i}{A_i - 1}\theta_j^2, \tag{15}$$

In Eq. (13), $\psi(10\,\mathrm{fm})$ is the radial amplitude at $r = 10$ fm:

$$\rho_j(10\,\mathrm{fm}) = \psi_j^2(10\,\mathrm{fm}). \tag{16}$$

In our case where ℓ=1, $J_i = 3/2$, $J_f = 2$ and $I = 1, 2$, the transformation coefficients are $\alpha_{1,3/2}$=$\alpha_{2,3/2}$=$\alpha_{2,1/2}$=$1/\sqrt{2}$ and $\alpha_{1,1/2}$=-$1/\sqrt{2}$. In addition, to a good approximation, $\psi_{1/2}(10\,\mathrm{fm}) = \psi_{3/2}(10\,\mathrm{fm}) = \psi(10\,\mathrm{fm})$. Hence Eq. (11) simplifies to:

$$S_{17}(20\,\mathrm{keV}) = 2.99{\cdot}10^6\,\rho(10\,\mathrm{fm})\,S, \tag{17}$$

where $S = S_{3/2} + S_{1/2}$.

In Table III we give the values of θ_j obtained from 0p shell model calculations with a variety of interactions [29,30,31] which are appropriate for the lower part of the 0p shell. These amplitudes are quite stable with respect to a reasonable range of interactions.

In Table IV we compare the theoretical spectroscopic factors with those obtained from reaction data [15] for states of ^{8}Li as well as those extracted from the observed widths of unbound states in ^{8}Li and ^{8}B. [32] The spectroscopic factors for the unbound states are obtained from $\Gamma_{exp} = S\,\Gamma_{sp}$ where Γ_{sp} is the single-particle width for a resonance at the experimental separation energy in the our potential geometry ($R = 2.40$ fm and $a = 0.62$ fm). The decay data are observed to be in excellent agreement with theory. The reaction spectroscopic factor for the 2^+ state is low with respect to theory, however, it depends upon the potential parameters used for the DWBA calculations. The DWBA fits to the data shown in Ref 15 are not particularly good, and we would suggest an new look at the analysis of this data as well as experimental confirmation. In the meantime we adapt the theoretical spectroscopic factors.

Combining with our results of $S = 1.15 \pm 0.05$ and $\rho(10\,\mathrm{fm}) = (7.0 \pm 0.8){\cdot}10^{-6}$ fm^{-3} we obtain $S_{17}(20\,\mathrm{keV}) = 24.1 \pm 2.9$ eV-barns.

IV. RELATIONSHIP TO THE ^{7}LI(N,γ)^{8}LI CROSS SECTION

Barker[33] has pointed out that standard potential models tend to overestimate the experimentally well-determined low-energy ^{7}Li(n,γ)^{8}Li cross section. He argued, that one should modify either the potential parameters or the spectroscopic factor to get agreement with experiment. To study this issue, we performed calculations for the ^{7}Li(n,γ)^{8}Li reaction.

Because there is no Coulomb barrier in this reaction, the inner parts of the wave functions have the same importance as the asymptotic parts. Thus the cross section does not depend solely on the asymptotic normalization of the bound state wave function. For the ^{8}Li bound state we used the same potential parameters as for ^{8}B, except a change in the potential depth to get the exact neutron separation energy of 2.033 MeV. For the ^{7}Li+n scattering states, we modify the potentials to reproduce the experimental scattering lengths of the $I = 1$, and $I = 2$ channel spin states, respectively.[33]

The thermal ^{7}Li(n,γ)^{8}Li cross section obtained with our potential parameters is 76 mb. The range of potential values allowed by our analysis would change this only by about 5 percent. The experimental thermal cross section is 45.4$\pm$3.0 mb.[32] Thus we also obtain an overestimation of the ^{7}Li(n,γ)^{8}Li cross section as did Barker. He concluded that either the potential parameters or the spectroscopic factor has to be changed in order to agree with the experiment, and that these changes would bring the ^{7}Be(p,γ)^{8}B S_{17}(20 keV) factor down to 16-17 eV-barns. The modifications to the potential are very large (R is changed from 2.39 to 1.01 fm or a is change from 0.65 fm to 0.27 fm) and we can see from Figs. 1$-$2 that these large changes are inconsistent with the Coulomb displacement energy. Thus we can exclude the possibility of radically changing the potential parameters. In the spirit of Ref 33, the only remaining possibility would be the reduction of the spectroscopic factor to about 0.71. But given the general agreement we obtain for the decay widths in Table IV, such a large change in the spectroscopic factor seems unreasonable. In fact such a drastic change would question the adequacy of the potential model itself.

We would like to point out that the discrepancy in the ^{7}Li(n,γ)^{8}Li cross section could

be resolved in a way which does not affect the ^{7}Be(p,γ)^{8}B cross section. As mentioned, contrary to ^{7}Be(p,γ)^{8}B, the inner part of the wave functions is important in the case of ^{7}Li(n,γ)^{8}Li. Although the reproduction of the scattering lengths fixes the external part of the scattering wave functions, the internal, off-shell, part is not well-constrained. For instance, if the inner node of the wave function were somewhat further outside than in the potential model, this would bring the ^{7}Li(n,γ)^{8}Li cross section down. To illustrate that the node position is not well-defined, we show in Fig. 4 the inner part of the $I = 2$ scattering wave function of the standard potential (BI) of Barker[33] (solid line) together with the scattering state obtained from the cluster model of Ref 34 (dashed line) at E_{CM}=10 keV. This change in the off-shell behavior is enough to reduce the ^{7}Li(n,γ)^{8}Li cross section considerably. In fact, the dashed line of Fig. 4, together with the bound state of the standard potential of Barker[33] results (after a $1/v$ extrapolation from 10 keV) in a thermal cross section of 46.3 mb, which is close to the experimental value. We emphasize again, that this modification in the off-shell behavior of the scattering wave functions has no effect on the ^{7}Be(p,γ)^{8}B cross section.

V. RELATION TO THE ^{8}B QUADRUPOLE MOMENT

The quadrupole moment, Q, of ^{8}B is related to the above calculations in the following way. Q is proportional to the matrix element of the $E2 = r^2Y^{(2)}$ one-body operator whose reduced matrix element is given by a summation over products of many-body matrix elements times single-particle matrix elements[35]:

$$\langle J_i \,||\, E2 \,||\, J_i \rangle = \sum_{j,j',t_z} \frac{\langle J_i \,||\, [a^\dagger_{j,t_z} \otimes \tilde{a}_{j',t_z}]^{(\lambda)} \,||\, J_i \rangle}{\sqrt{2\lambda+1}} \langle j, t_z \,||\, E2 \,||\, j', t_z \rangle, \qquad (18)$$

where λ=2. The t_z indicates a sum over protons and neutrons. By inserting a complete set of states[36] (J_f) of the $A = 7$ system between the a^+ and $\tilde{a}$, one can rewrite this as a sum over all 0p shell states of the A=7 system:

$$\langle J_i \,||\, E2 \,||\, J_i \rangle = (2J_i+1) \sum_{j,j',t_z,J_f} (-1)^{J_f+j'} \theta_{j,t_z}(J_i,J_f)\theta_{j',t_z}(J_i,J_f)$$
$$\times \left\{ \begin{array}{ccc} J_i & J_i & 2 \\ j & j' & J_f \end{array} \right\} \langle j,t_z \,||\, E2 \,||\, j',t_z \rangle, \qquad (19)$$

where the states J_f are in ^{7}Be for t_z=proton and are in ^{7}B for t_z=neutron. The sum over J_f can be broken down into the term coming from the ground state of ^{7}Be (referred to as the valence term, vp) and all other terms coming from excited states in ^{7}Be and all states in ^{7}B (referred to as 0p core proton and neutron terms, pcp and pcn, respectively). The single-particle matrix elements are given by a geometrical term times the single-particle mean-square radius, $\langle r^2 \rangle$.[35] The Q moment can thus be expressed in the form

$$Q(^8\mathrm{B}) = -0.80\,\theta_{3/2}\theta_{1/2}\langle r^2\rangle_{vp}e_p + 0.203\,\langle r^2\rangle_{pcp}e_p + 0.183\,\langle r^2\rangle_{pcn}e_n$$
$$= 0.187\langle r^2\rangle_{vp}e_p + 0.203\,\langle r^2\rangle_{pcp}e_p + 0.183\,\langle r^2\rangle_{pcn}e_n, \qquad (20)$$

where the CKI interaction[29] was used for the spectroscopic factors. The numerical coefficient -0.80 is purely geometrical. The effective charges e_p and e_n take into account the non-0p parts of the wave functions which include 0s to 0p and 0p to 0d1s proton excitations. For the remaining discussion we will use values of $e_p = 1.35e$ and $e_n = 0.35e$,[35] although we realize that these are approximate values and that they may depend upon the binding energy.[37] Our calculation for the radial matrix elements gives $\langle r^2\rangle_{vp} = 19.7$ fm^2, $\langle r^2\rangle_{pcp} = 8.1$ fm^2, and $\langle r^2\rangle_{pcn} = 7.8$ fm^2, and hence we obtain $Q(^8\mathrm{B}) = 7.7\ e\,\mathrm{fm}^2$, in reasonable agreement with the experimental value[10] of $6.83\pm0.21\ e\,\mathrm{fm}^2$. The Q moment for ^{8}Li can be obtained by interchanging the labels for p and n in Eq. (20), and using our value of $\langle r^2\rangle_{vn} = 13.3$ fm^2, to obtain $Q(^8\mathrm{Li}) = 3.42\ e\,\mathrm{fm}^2$ which is close to the experimental value[10] of $3.27\pm0.06\ e\,\mathrm{fm}^2$. The effective charges we use are approximate, and it would very difficult to estimate the them more quantitatively. Even though our calculated values are close to the experimental values, it is clear that the relationship to the valence rms radius and asymptotic normalization is

quite complicated. In addition, we note that the Q moment depends upon the interference term $\theta_{3/2}\theta_{1/2}$ whereas the tail density is determined by the combination $A_{3/2}^2 + A_{1/2}^2$ which is dominated by $\theta_{3/2}$. The term in Eq. (19) which is proportional to $\theta_{3/2}\theta_{3/2}$ is zero because the 6j symbol vanishes (physically it is related to the vanishing of the Q moments in the middle of a single j shell).

VI. RADIAL DENSITIES AND MOMENTUM DISTRIBUTIONS

The radial densities obtained in our potential parameters are shown in various ways in Figs. 5-7. For the sake of simplification it will be assumed in this section that there is a single valence proton with a binding energy of 0.138 MeV, four tightly bound core protons (two in the 0p shell with a separation energy of about 6 MeV and two in the 0s shell with a separation energy of about 16 MeV) and three tightly bound neutrons (one on the 0p shell with a separation energy of about 8 MeV and two in the 0s shell with a separation energy of about 18 MeV). The actual situation is a little more complicated than this because $S = 1.15$ and because there is also some parentage of the protons in ^{8}B to the first excited state in ^{7}Be which will result in some leakage of the core protons to larger radii. The results here are thus more qualitative than those given above for S_{17}.

The normal density $\rho(r)$ is shown in Fig. 5, the probability density $P(r) = 4\pi r^2\rho(r)$ on a log scale in is shown Fig. 6, and the probability density on a linear scale is shown Fig. 7. In all figures the neutron density is shown by the dashed line, the core proton density with crosses, and the valence proton density with a solid line. Note in Figs. 6–7 that the areas are equal to three, four and one, respectively. The valence proton clearly has a large extension, but whether or not it constitutes a "halo" or a "skin" is a question of semantics.

The valence proton (vp), core proton (cp) and neutron (n) rms radii are:

$$\sqrt{\langle r^2\rangle_{vp}} = 4.44\,\mathrm{fm}, \tag{21}$$

$$\sqrt{\langle r^2\rangle_{cp}} = 2.39\,\mathrm{fm}, \tag{22}$$

and

$$\sqrt{\langle r^2\rangle_{n}} = 2.21\,\mathrm{fm}. \tag{23}$$

The total proton rms radius is given by

$$\sqrt{\langle r^2\rangle_{p}} = \sqrt{[4\langle r^2\rangle_{cp} + \langle r^2\rangle_{vp}]/5} = 2.92\,\mathrm{fm}. \tag{24}$$

The rms charge radius includes the rms radius of 0.80 fm for the proton:

$$\sqrt{\langle r^2\rangle_{ch}} = \sqrt{[\langle r^2\rangle_{p} + 0.64\mathrm{fm}^2]} = 3.03\,\mathrm{fm}, \tag{25}$$

and the matter radius is given by:

$$\sqrt{\langle r^2\rangle_{m}} = \sqrt{[5\langle r^2\rangle_{p} + 3\langle r^2\rangle_{n}]/8} = 2.68\,\mathrm{fm}. \tag{26}$$

Our results can be compared to those of other theoretical calculations. The results of $\sqrt{\langle r^2\rangle_{vp}} = 3.75$ fm obtained by Riisager and Jensen [38] is much smaller than ours but they use an arbitrary potential shape. The reason for their small S_{17} is obvious from Fig. 3. The calculations presented in Ref 10 for the Q moment appear to be very close to our results.

The high-energy (800 MeV/nucleon) interaction cross sections for ^{8}B and ^{8}Li on ^{12}C have been calculated with the method of Ref 39. The results with the finite-range interaction are σ=843 mb for ^{8}B and σ=820 mb for ^{8}Li. These can be compared to the experimental values of σ=784(14) mb [9] for ^{8}B and σ=768(9) mb [40] for ^{8}Li. The agreement for the magnitudes is as good as can be expected from the uncertainties in the calculation. However, the ^{8}B/^{8}Li ratio (in which some of the reaction uncertainties may cancel) is in excellent agreement between theory and experiment. The effects of the proton "halo" in ^{8}B and the neutron "halo" in ^{8}Li are not large compared with the classic cases [39,40] of ^{11}Li, ^{11}Be

and ^{14}Be. The low-energy (20-60 MeV/nucleon) total reaction cross section appears to be more sensitive to the extended proton distribution in ^{8}B.[41]

Recent radioactive beam experiments[11,42] have looked at the momentum distribution of the ^{7}Be fragments which result from the break-up of a beam ^{8}B on various targets. From these experiments one expects to determine the momentum distribution of the most loosely bound protons. The longitudinal momentum $P(k_z)$ obtained for the valence proton is shown in Fig. 8. This is obtained by the Fourier transform of the spatial wave function:

$$\tilde{\Psi}(\vec{k}) = \frac{1}{(2\pi)^{3/2}} \int \Psi(\vec{r}) e^{i\vec{k}\cdot\vec{r}} d^3r. \tag{27}$$

where $\Psi(\vec{r}) = \psi(r)Y_\ell(\hat{r})$, $\tilde{\Psi}(\vec{k}) = \tilde{\psi}(k)Y_\ell(\hat{k})$, and where the radial momentum distribution is given by:

$$\tilde{\psi}(k) = \sqrt{\frac{2}{\pi}} \frac{i^{-\ell}}{k} \int \psi(r) j_\ell(kr) r^2 \, dr. \tag{28}$$

The longitudinal momentum distribution is given by

$$P(k_z) = \frac{1}{2} \int |\tilde{\psi}(k)|^2 \, k_r dk_r, \tag{29}$$

where $k^2 = k_r^2 + k_z^2$.

The calculated momentum distribution has a width of about 150 MeV/c compared to the experimental value of 81±6 MeV/c. Given the good agreement generally found for calculated and observed neutron halos[43] this disagreement is puzzling. There is some discussion in the literature about ways to improve the above calculation to take into account the peripheral nature of the reaction.[43,44] In the peripheral direct reaction model one puts in an additional cut-off in Eq. (29) to exclude the interior part of the radial distribution which presumably does not contribute because the cross section coming from that part is dominated by a more violent reaction where the core (^{7}Be in this case) is destroyed. We have phenomenologically modeled this effect by putting a Fermi shaped cut-off factor in Eq. (28) which has the effect of excluding the interior out to a radius R_{cut} and with a diffuseness

a_{cut}. We take a_{cut}=0.65 fm and vary R_{cut} to get about the observed momentum distribution. This requires R_{cut}=5 fm and the results are shown by the dashed line in Fig. 8. The cut-off results in a reduction of $P(k_z)$ at small momenta by a factor of 2.5 and we have renormalized the cut-off distribution by this factor in order to show the change in width. It is already known that the cut-off factor does not have much effect on the neutron halo momentum distributions,[43] and we have demonstrated that even a value as large as R_{cut} = 5 fm has little effect on the width of the ^{11}Be neutron halo momentum distribution. We do not know why we should need R_{cut}=5 fm, but we note that this corresponds to the point in Fig. 5–7 where the valence proton density falls below the core density. More work needs to be done to understand these results.

Schwab et al.[11] present an RPA calculation which goes beyond the 0p shell and which agrees with the shape of the observed momentum distribution. However, the shape of the wave function beyond about 6 fm as shown in Fig. 4 in their paper appears unrealistic to us. The shape beyond about 6 fm is entirely determined by the Coulomb and centrifugal barriers, and their shape differs from this expectation. Our own calculation can of course be criticized for staying within the 0p shell. However, a very recent "no-core" calculation[45] along the lines of those given in Ref 46 which takes into account the lowest six major shells (21 shell-model orbitals) and up to $4\hbar\omega$ in excitation gives spectroscopic factors which are close to the present 0p shell results.

VII. CONCLUSIONS

Our calculated value of $S_{17}(20\,\mathrm{keV}) = 24.1 \pm 2.9$ eV-barns is in consistent on the upper side with the values of 25-27 eV-barns inferred from the (p,γ) data of Parker[4] and Kavanagh et al.,[5] and on the lower side with the value obtained from the weighted average of all experimental data, $S_{17} = 22.2 \pm 2.3$ eV-barns,[47] which is the value currently adopted in most solar models.[48] As far as other theoretical predictions are concerned, our current result for S_{17} is in the middle of the range of (~30 eV-barns)[49] to (~17 eV-barns).[26,50]

We note, that in contrast to the common belief (e.g. Ref 50), a small value of S_{17} does not make the solar neutrino problem less severe. If one takes standard nuclear and solar physics, and standard neutrino properties, then the best fit [51] of the neutrino fluxes indicates a suppression in both the ^{7}Be (ϕ_7) and the ^{8}B (ϕ_8) neutrino fluxes, but the suppression is *much* stronger in ϕ_7. However, a smaller S_{17} value *alone* would make the predicted ϕ_7/ϕ_8 ratio larger, which would make the solar neutrino problem even worse.

Acknowledgements

We would like to acknowledge support from NSF grants 94-03666 and 92-53505. Also we thank Sam Austin and Gregers Hansen for their helpful comments.

Figure Captions

Fig. 1: The valence proton rms radius as a function of Δ_o. The three lines join the points obtained for different value of the diffuseness a for R=2.0 fm (filled circles), R=2.4 fm (open circles) and R=2.8 fm (squares). The results for the specific potentials in Table II are shown by the labeled crosses. The region between the vertical lines are the range of values allowed by the displacement energy.

Fig. 2: The valence proton density at r=10 fm as a function of Δ_o (see caption to Fig. 1).

Fig. 3: The valence proton density at r=10 fm as a function of the valence proton rms radius (see caption to Fig. 1).

Fig. 4: The scattering wave function for ^{7}Li(n,γ) obtained with the standard potential (BI) of Barker[33] (solid line) together with the results obtained with the cluster model[34] (dashed line).

Fig. 5: The radial density profile for ^{8}B for the neutrons (dashed line), the core protons (crosses) and the valence proton (solid line).

Fig. 6: The radial probability distribution for ^{8}B on a log scale (see caption to Fig. 5).

Fig. 7: The radial probability distribution for ^{8}B on a linear scale (see caption to Fig. 5).

Fig. 8: The momentum distribution for the ^{8}B valence proton. The solid line corresponds to the full radial wave function and the dashed line corresponds to the radial wave function cut-off at r=5 fm.

TABLES

TABLE I. Values of Δ_o, the rms proton radius and $\rho(10\,\text{fm})$ as a function of R and a.

spin-orbit	R (fm)	a (fm)	Δ_o (MeV)	rms (fm)	$\rho(10\,\text{fm})\cdot 10^6$ (fm^{-3})
yes	2.0	0.4	2.108	3.70	4.25
yes	2.0	0.6	1.947	4.14	5.81
yes	2.0	0.8	1.786	4.62	8.00
yes	2.4	0.4	1.969	4.02	5.27
yes	2.4	0.6	1.840	4.40	6.85
yes	2.4	0.8	1.705	4.84	9.07
yes	2.8	0.4	1.836	4.35	6.48
yes	2.8	0.6	1.735	4.68	8.10
yes	2.8	0.8	1.623	5.08	10.40
no	2.4	0.4	1.991	3.97	5.09
no	2.4	0.6	1.851	4.38	6.74
no	2.4	0.8	1.708	4.84	9.05

TABLE II. Woods-Saxon potential parameters from the present analysis compared to those used by Tombrello[52] and Barker I.[33] Barker II and III correspond to those values Barker needed to reproduce the ^{7}Li(n,γ) cross section.

Set	R (fm)	a (fm)
Present	2.40	0.62
Tombrello (T)	2.95	0.52
Barker BI	2.39	0.65
Barker BII	1.01	0.65
Barker BIII	2.39	0.27

TABLE III. Spectroscopic amplitudes $\theta_j(J_i, J_f = 3/2)$ for ^{8}B to ^{7}Be from the CKI,[29] Kumar[30] and PTBME[31] interactions. The order of the states for a given J_f^π is indicated by n_f.

J_f^π, n_f	j	CKI	Kumar	PTBME
2^+,1	3/2	0.988	0.966	0.986
	1/2	−0.237	−0.259	−0.253
1^+,1	3/2	0.567	0.606	0.552
	1/2	−0.352	−0.244	−0.342
3^+,1	3/2	0.581	0.555	0.565
1^+,2	3/2	0.617	0.574	0.525
	1/2	0.840	0.861	0.859

TABLE IV. Theoretical spectroscopic factors $S = S_{1/2} + S_{3/2}$ for ^{8}Li and ^{8}B compared to those based upon decay widths[32] and (d,p) reaction data.[15]

J_f^π	$^8B_{exp}$(decay)	$^8Li_{exp}$(decay)	$^8Li_{exp}$(reaction)	CKI	Kumar	PTBME
2^+			0.87(13)	1.17	1.14	1.19
1^+	0.54(7)		0.48(7)	0.51	0.49	0.47
3^+	0.38(4)	0.41(7)		0.39	0.35	0.36

1. B. T. Cleveland, T. Daily, R. Davis, J. Distel, K. Lande, C. K. Lee, P. Wildenhain, and J. Ullman, Nucl. Phys. B (Proc. Suppl.) **38**, 47 (1995).
2. Y. Suzuki, Nucl. Phys. B (Proc. Suppl.) **38**, 54 (1995).
3. J. N. Bachall and R. K. Ulrich, Rev. Mod. Phys. **60**, 297 (1988).
4. P. D. Parker, Phys. Rev. **150**, 851 (1966).
5. R. W. Kananagh, T. A. Tombrello, T. A. Mosher and D. R. Goosman, Bull. Am. Phys. Soc. **14**, 1209 (1969); R. W. Kavanagh, *Cosmology, Fusion and other Maters* (Colorado Assoc. Univ. Press, Boulder, 1972), p. 169.
6. B. W. Filippone, S. J. Elwyn, C. N. Davids and D. D. Koertke, Phys. Rev. Lett. **50**, 412 (1983); Phys. Rev. C **28**, 2222 (1983).
7. F. J. Vaugn, R. A. Chalmers, D. Kohler and L. F. Chase Jr., Phys. Rev. C **2**, 1657 (1970).
8. T. Motobayashi et al., Phys. Rev. Lett. **73**, 2680 (1994).
9. I. Tanihata et al., Phys. Lett. B **206**, 592 (1988); Nucl. Phys. **A520**, 411c (1990).
10. T. Minamisono et al., Phys. Rev. Lett. **69**, 2058 (1992).
11. W. Schwab et al. Z. Phys. A **350**, 283 (1995).
12. J. A. Nolen and J. P. Schiffer, Ann. Rev. Nucl. Sci. **19**, 471 (1969).
13. S. Schlomo, Rep. Prog. Phys. **41**, 957 (1978).
14. R. Sherr and G. Bertsch, Phys. Rev. C **32**, 1809 (1985).
15. J. P. Schiffer, G. C. Morrison, R. H. Siemssen and B. Zeidman, Phys. Rev. **164**, 1274 (1967).
16. G. B. Liu and H. T. Fortune, Phys. Rev. C **38**, 1985 (1988).
17. W. E. Ormand and B. A. Brown, Nucl. Phys. **A491**, 1 (1989).
18. H. de Vries et al., Atomic Data and Nuclear Data Tables, **36**, 3 (1987).
19. R. H. Bassel, B. A. Brown, R. Lindsay and N. Rowley, J. Phys. **G8**, 1215 (1982).
20. T. Suzuki, H. Sagawa and A. Arima, Nucl. Phys. **A536**, 141 (1992).
21. A. Johansson, U. Svandberg, and P. E. Hodgson, Ark. Fys. **19** 541 (1961).
22. A. Aurdal, Nucl. Phys. **A146**, 385 (1970).

23. R. G. H. Robertson, Phys. Rev. C **7**, 543 (1973).

24. K. H. Kim, M. H. Park, and B. T. Kim, Phys. Rev. C **35**, 363 (1987).

25. R. F. Christy and I. Duck, Nucl. Phys. **24**, 89 (1961); R. D. Williams and S. E. Koonin, Phys. Rev. C **23**, 2773 (1981).

26. A. M. Mukhamedzhanov and N. K. Timofeyuk, JETP Lett. **51**, 282 (1990); H. M. Xu, C. A. Gagliardi, R. E. Tribble, A. M. Mukhamedzhanov, and N. K. Timofeyuk, Phys. Rev. Lett. **73**, 2027 (1994).

27. We use the reduced matrix element convention of A. R. Edmonds, *Angular Momentum in Quantum Mechanics*, (Princeton University Press, 1957).

28. A. E. L. Dieperink and T. de Forest, Phys. Rev. C **10**, 543 (1974).

29. S. Cohen and D. Kurath, Nucl. Phys. **A73**, 1 (1965).

30. N. Kumar, Nucl. Phys. **A235**, 221 (1974).

31. R. E. Julies, W. A. Richter and B. A. Brown, S. Afr. J. Phys. **15**, 35 (1992).

32. F. Ajzenberg-Selove, Nucl. Phys. **A490**, 1 (1988); we use $\Gamma(3^+,{}^8\mathrm{Li})$=33(6) keV from Table 8.2, the $S_{exp}({}^8\mathrm{Li})$ from page 82 section 8, $\Gamma(1^+,{}^8\mathrm{B})$=37(5) keV and $\Gamma(3^+,{}^8\mathrm{B})$=350(40) keV from Table 8.9.

33. F. C. Barker, Aust. J. Phys. **33**, 177 (1980).

34. A. Csótó, K. Langanke, S. E. Koonin, and T. D. Shoppa, Phys. Rev. **C52**, 1130 (1995).

35. M. Carchidi, B. H. Wildenthal and B. A. Brown, Phys. Rev. C **34**, 2280 (1986).

36. D. J. Millener, D. E. Alburger, E. K. Warburton and D. H. Wilkinson, Phys. Rev. C **26**, 1167 (1982).

37. B. A. Brown, A. Arima and J. B. McGrory, Nucl. Phys. **A277**, 77 (1977).

38. K. Riisger and A. S. Jensen, Phys. Lett. B **301**, 6 (1993).

39. G. F. Bertsch, B. A. Brown and H. Sagawa, Phys. Rev. C **39**, 1154 (1989).

40. I. Tanihata et al., Phys. Rev. Lett. **55**, 2676 (1985).

41. R. E. Warner et al., Phys. Rev. C **52**, R1166 (1995).

42. J. H. Kelley et al., Bull. Am. Phys. Soc. **40**, 978 (1995).

43. H. Sagawa and N. Takigawa, Phys. Rev. C **50**, 985 (1994).

44. H. Sagawa and K. Yazaki, Phys. Lett. B **244**, 149 (1990).

45. D. C. Zheng, B. A. Brown and B. R. Barrett, unpublished.

46. D. C. Zheng, J. P. Vary and B. R. Barrett, Phys. Rev. C **50**, 2841 (1994).

47. C. W. Johnson, E. Kolbe, S. E. Koonin, and K. Langanke Astrophys. J. **392**, 320 (1992).

48. J. N. Bahcall and M. H. Pinsonneault, Rev. Mod. Phys. **64**, 885 (1992).

49. P. Descouvemont and D. Baye, Nucl. Phys. **A567**, 341 (1994).

50. F. C. Barker and R. H. Spear, Astrophys. J. **307**, 847 (1986); F. C. Barker, Nucl. Phys. **A588**, 693 (1995).

51. S. Degl'Innocenti, G. Fiorentini, and M. Lissia, preprint INFNFE-10-94, submitted to Phys. Lett. B; V. Castellani, S. Degl'Innocenti, G. Fiorentini, M. Lissia, and B. Ricci, Phys. Rev. D **50**, 4749 (1994); V. Castellani, S. Degl'Innocenti, G. Fiorentini, and B. Ricci, preprint, to appear in the Proceedings of the Solar Modeling Workshop, Seattle, March, 1994.

52. T. A. Tombrello, Nucl. Phys. **71**, 459 (1965).

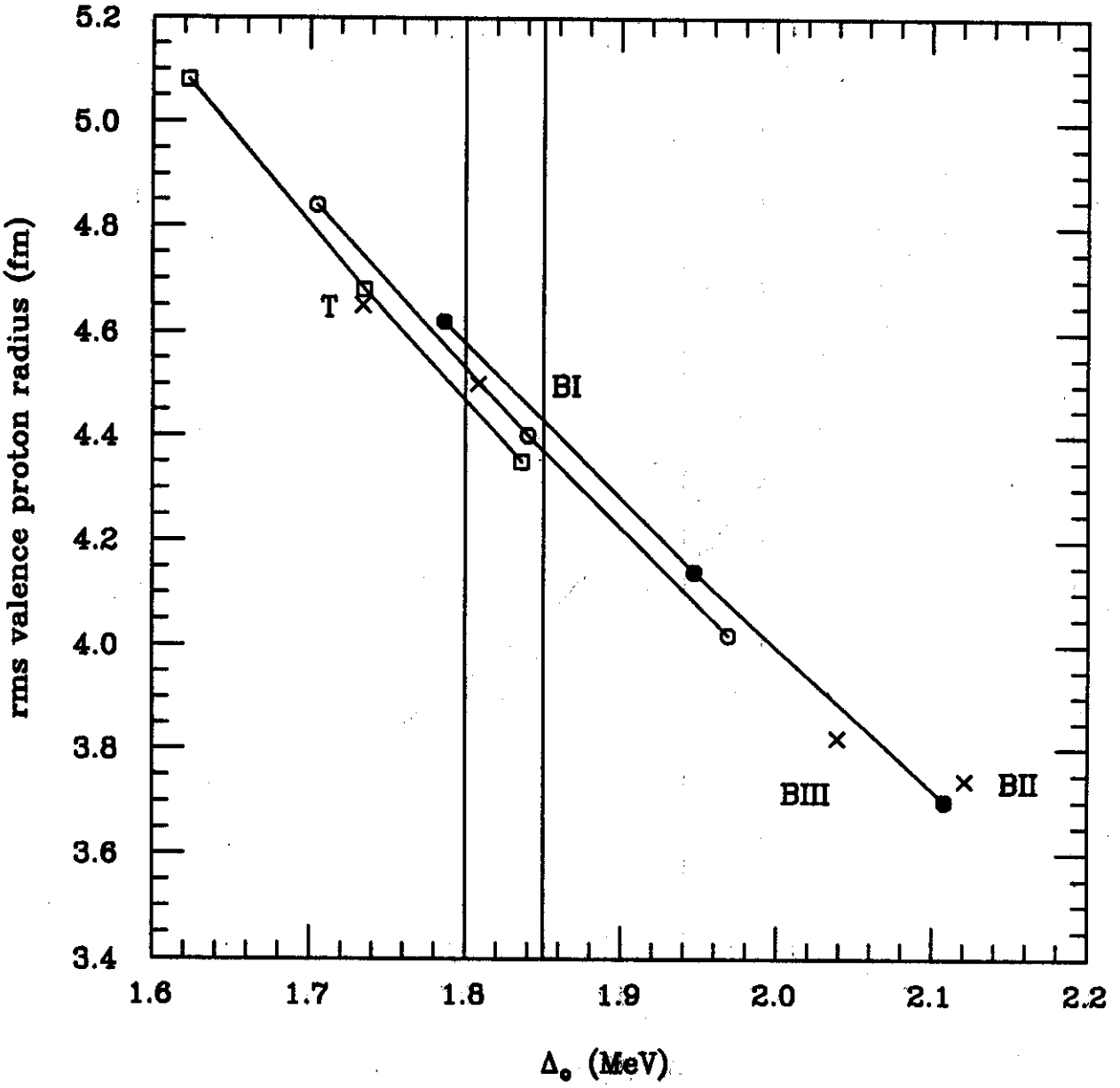
5.2
5.0
4.8
4.6
4.4
4.2
4.0
3.8
3.6
3.4
rms valence proton radius (fm)
1.6
1.7
1.8
1.9
2.0
2.1
2.2
Δ₀ (MeV)
T
BI
BII
BIII

FIGURE 1

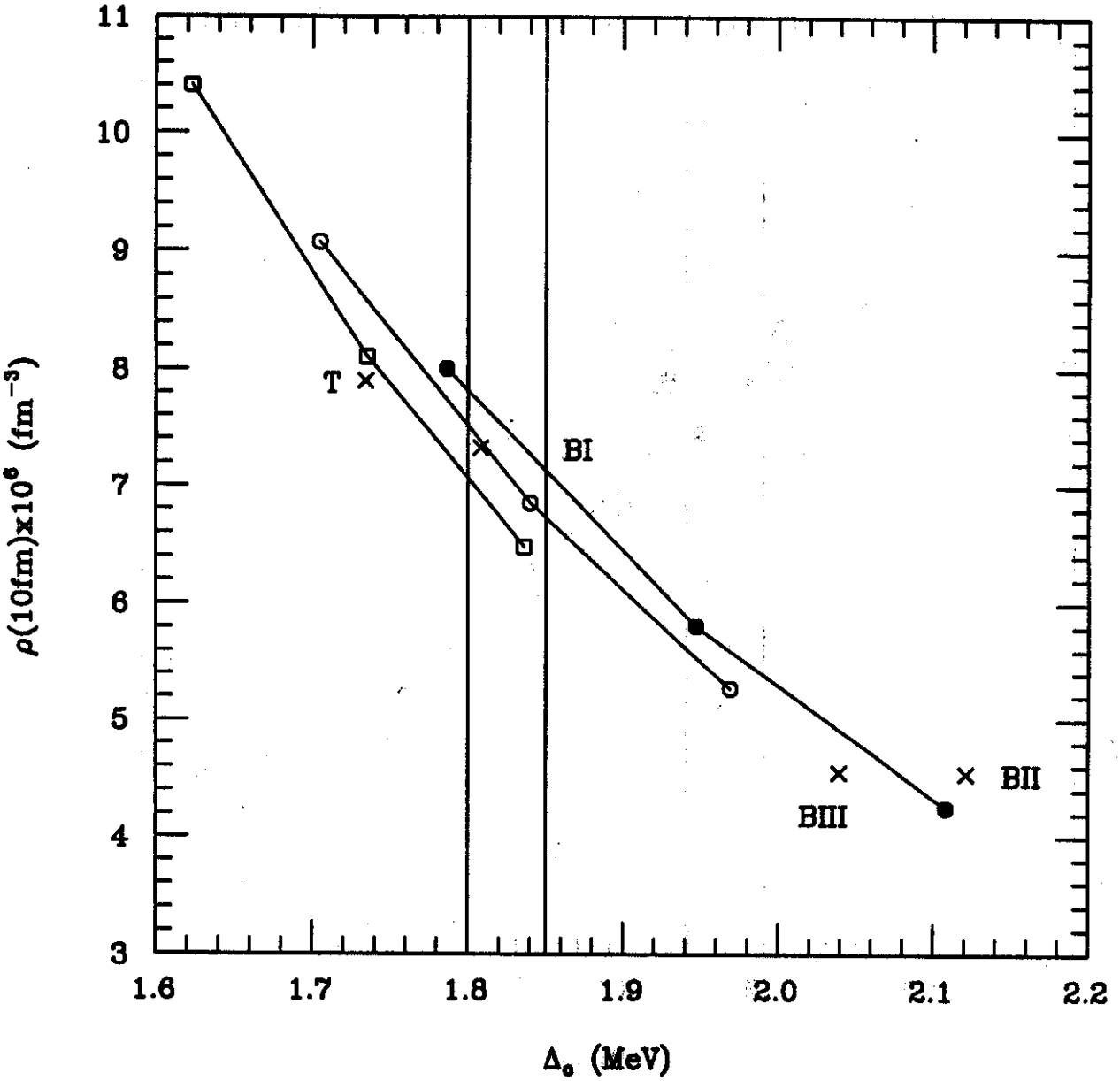
11
10
9
8
7
6
5
4
3
1.6
1.7
1.8
1.9
2.0
2.1
2.2
ρ(10fm)x10⁶ (fm⁻³)
Δ₀ (MeV)
T
BI
BII
BIII

figure 2

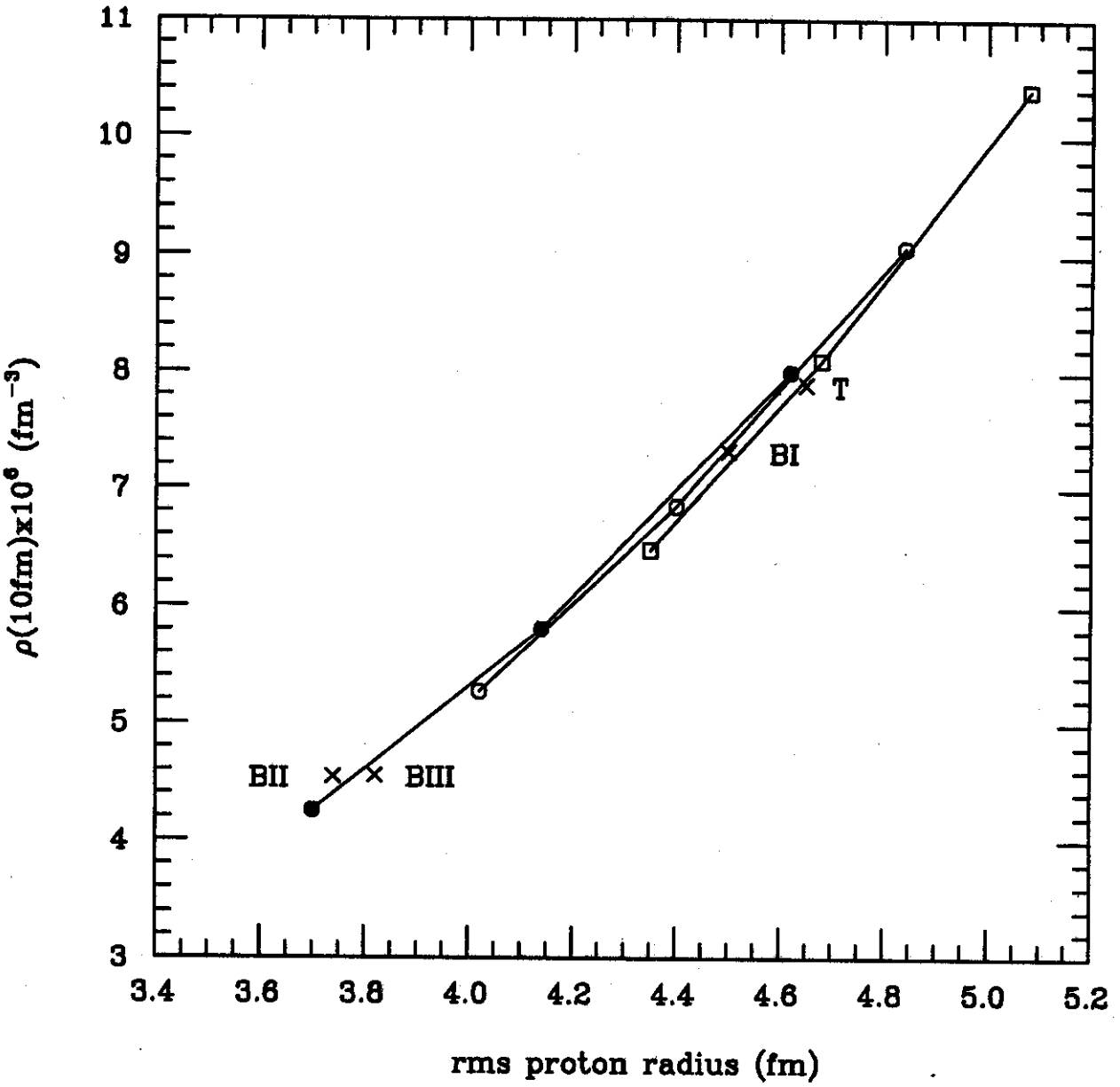
11
10
9
8
7
6
5
4
3
3.4
3.6
3.8
4.0
4.2
4.4
4.6
4.8
5.0
5.2
ρ(10fm)x10⁶ (fm⁻³)
rms proton radius (fm)
BII
BIII
BI
T

FIGURE 3

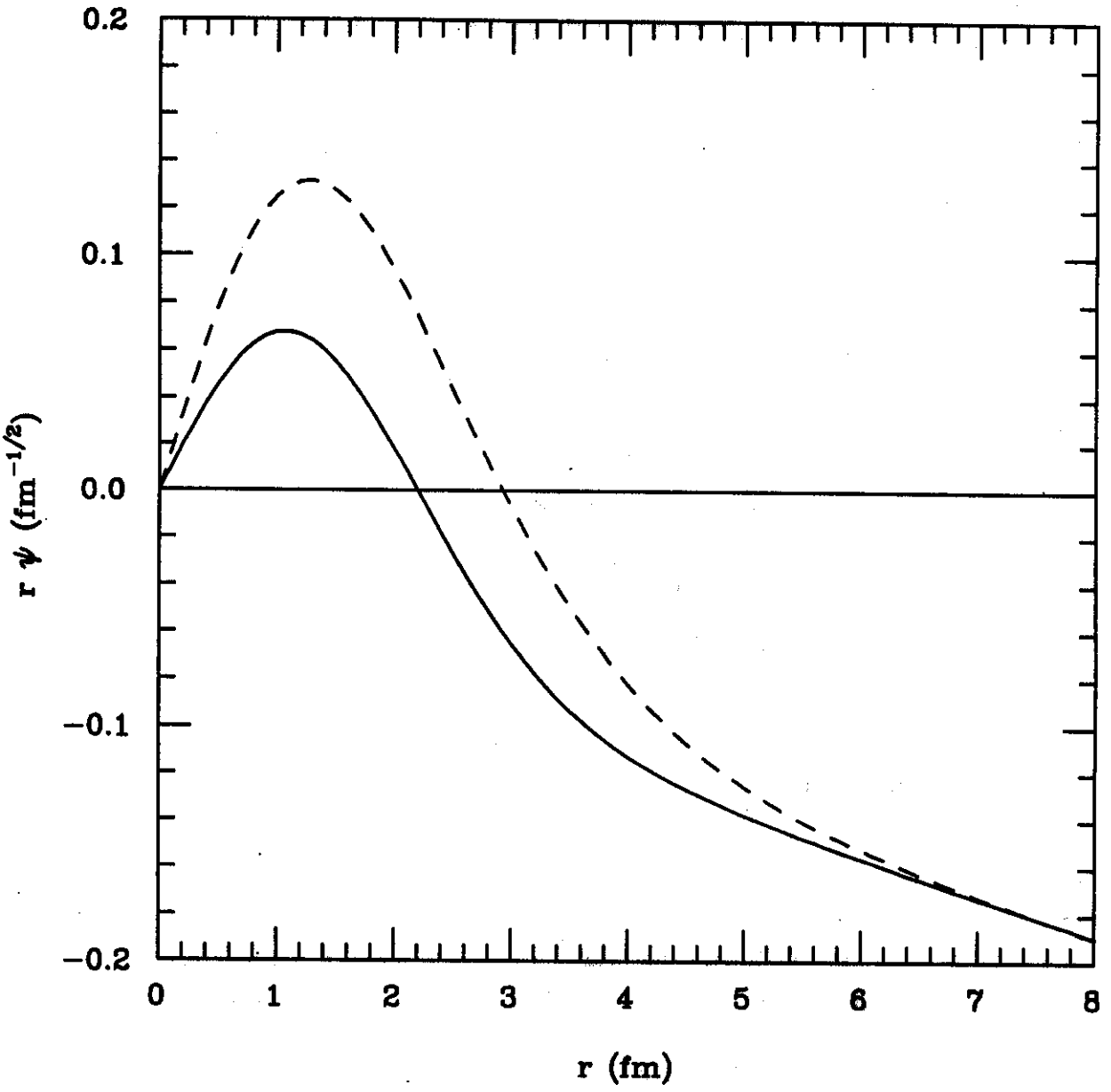

FIGURE 4

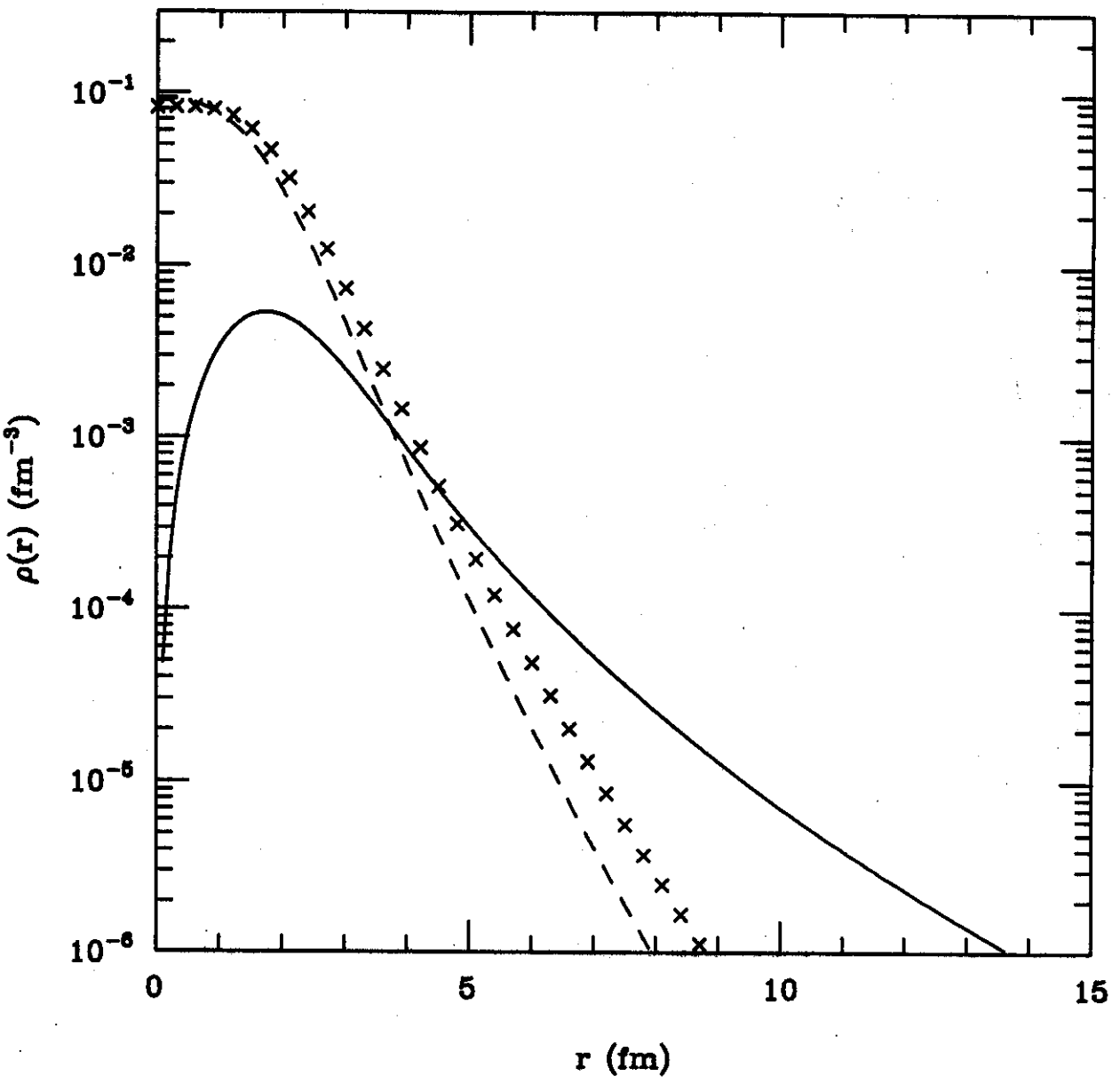

FIGURE 5

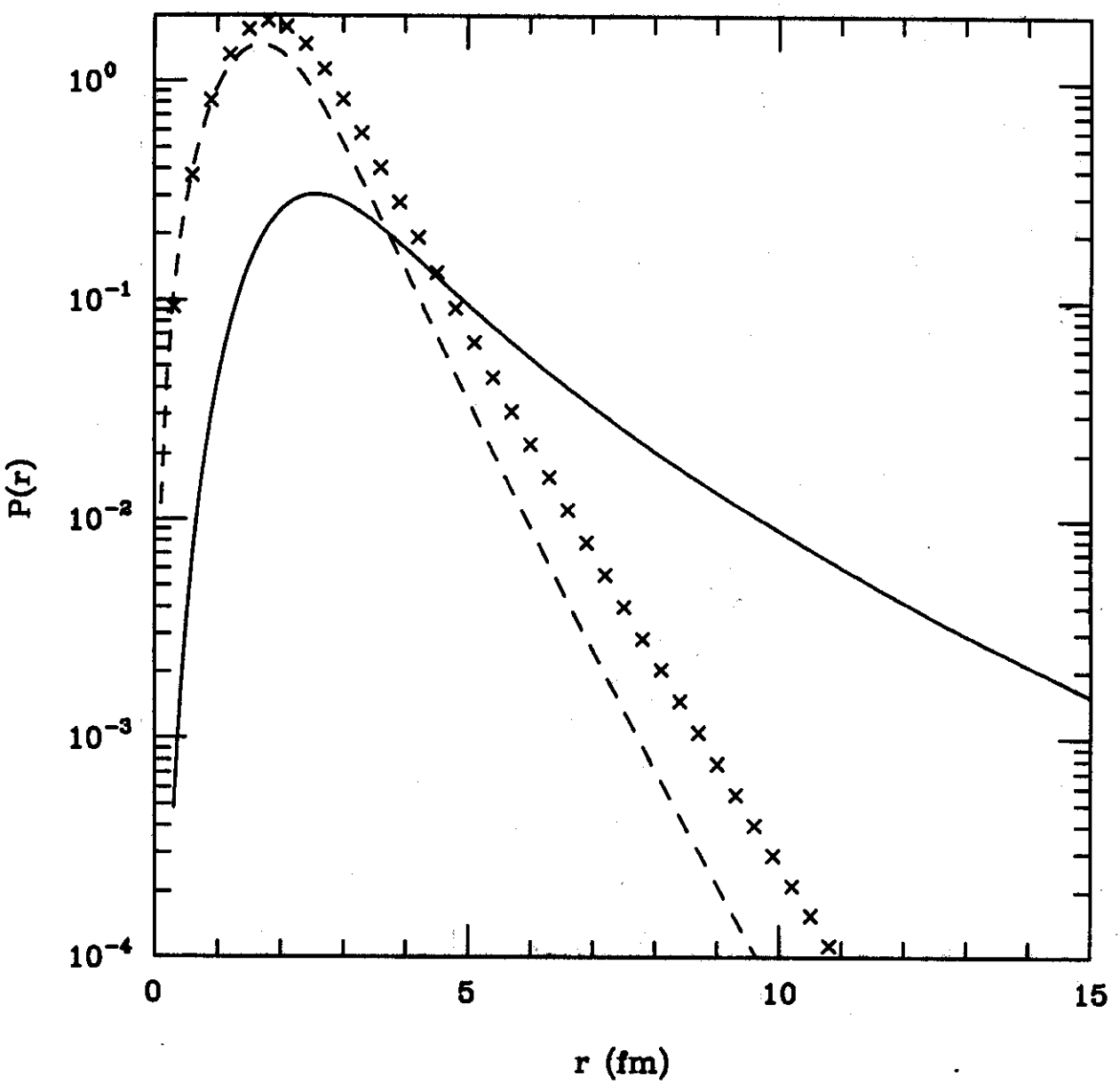

FIGURE 6

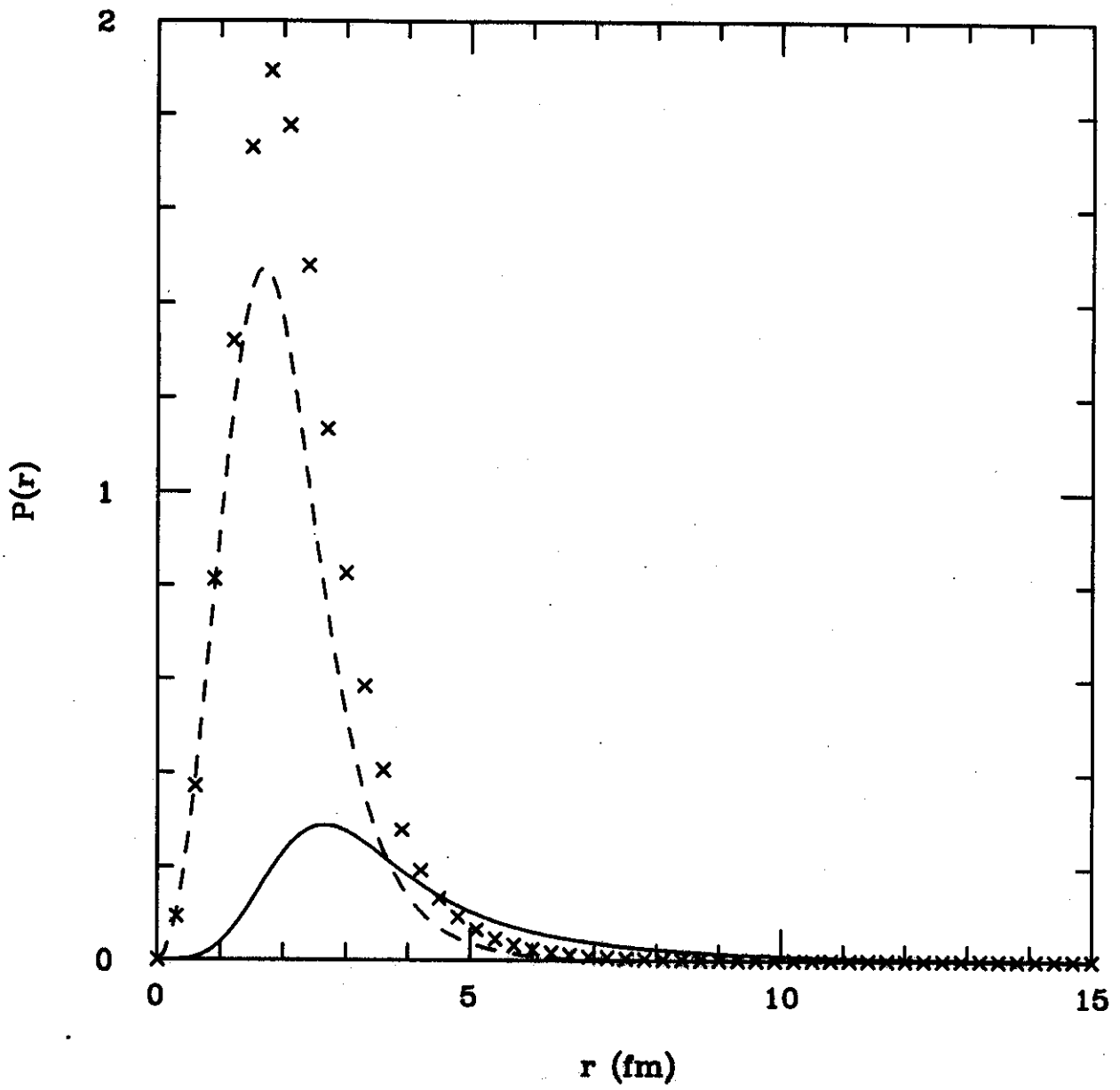

FIGURE 7

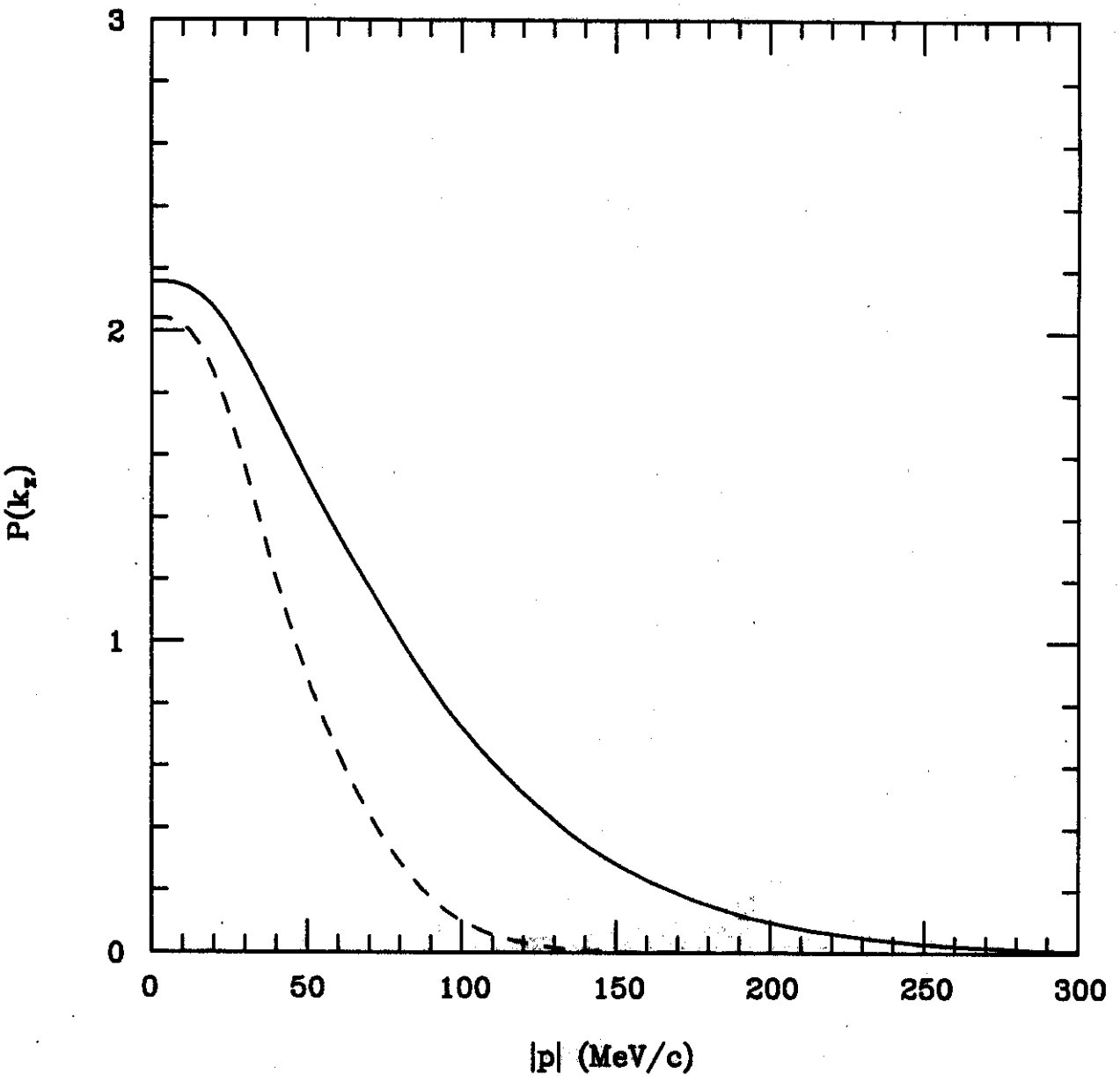

FIGURE 8